Identifying plausible historical scenarios for coupled lake level and seismicity rate changes: The case for the Dead Sea during the last two millennia.

Mariana Belferman[1], Amotz Agnon[2], Regina Katsman[1] and Zvi Ben-Avraham[1]

[1] *The Dr. Moses Strauss Department of Marine Geosciences, Leon H. Charney School of Marine Sciences, University of Haifa, Mt. Carmel, Haifa 3498838, Israel.*

[2] *The Fredy & Nadine Herrmann Institute of Earth Sciences, The Hebrew University of Jerusalem, Jerusalem 9190401, Israel*

Mariana Belferman: mkukuliev@gmail.com (corresponding author)

Amotz Agnon: amotz@huji.ac.il

Regina Katsman: rkatsman@univ.haifa.ac.il

Zvi Ben-Avraham: zviba@post.tau.ac.il

ABSTRACT

Seismicity triggered by water level changes in reservoirs and lakes is usually studied from well-documented contemporary records. Can such triggering be explored on a historical time scale when the data gathered on water level fluctuations in historic lakes and the earthquake catalogs suffer from severe uncertainties? These uncertainties stem from the different nature of the data gathered, methods, and their resolution. In this article, we show a way to considerably improve the correlation between interpolated records of historical water level reconstructions at the Dead Sea and discrete seismicity patterns in the area, over the period of the past two millennia. Inspired by the results of our previous study, we carefully revise the historical earthquake catalog in the Dead

Sea keeping only events with documented destruction in Jerusalem, the largest historical city in the vicinity of the lake. We then generate an ensemble of random interpolations of water level curves and rank them by correlation with the historical records of seismic stress release. We numerically simulate a synthetic catalog of earthquakes triggered by poroelastic deformations at hypocentral depths. The catalog is produced by a best-fit water level curve superimposed on the regional strike-slip tectonic deformations. The earthquakes of this synthetic catalog show an impressive agreement with historical earthquakes documented to damage Jerusalem. We demonstrate for the first time a high correlation between water level changes and the recorded recurrence intervals of historical earthquakes.

KEYWORDS

Seismic recurrence interval; Water level changes; Effective stress; Dead Sea

INTRODUCTION

Earthquakes induced by water level changes in lakes and reservoirs has been a focus of seismic investigations around the world (e.g. Simpson et al., 1988; Pandey and Chadha, 2003; Durá-Gómez and Talwani, 2010). Triggering is attributed to a drop in the effective normal stress at a fault, induced by water level change at the overlying lake's bed (Simpson et al., 1988; Durá-Gómez and Talwani, 2010; Hua et al., 2013b; Gupta, 2018). This kind of triggering may be particularly significant for areas with moderate and low tectonic strain accumulations (Pandey and Chadha, 2003; Gupta, 2018), such as the Dead Sea fault in the Middle East (e.g., Masson et al., 2015).

Seismic activity due to water level change was observed beneath artificial reservoirs immediately after their first filling (e.g., Simpson et al., 1988; Hua et al., 2013 a). It also appeared after several seasonal filling cycles (Simpson et al., 1988; Talwani, 1997), explained by diffusion of pore pressure to the earthquake's hypocentral depth via the fault (Durá-Gómez and Talwani, 2010). In addition, reservoir-induced seismicity sometimes manifests itself at long distances away from the reservoir (e.g., at 35 km, Durá-Gómez and Talwani, 2010). The correspondence of this kind of contemporary seismicity to water level change is usually identified based upon real-time data.

Alternatively, on a much longer time scale, changing seismic activity may also be associated with water level changes in historical water bodies (e.g., the Dead Sea, since 2 ka, Fig. 1A, in the Appendix, which occupies the tectonic depression along the Dead Sea fault). Water level hikes of ~15 m, characteristic for time intervals of centuries to millennia, were analyzed in Belferman et al. (2018) and shown to be able to moderate the seismicity pattern at the Dead Sea fault.

However, reconstruction of fluctuations in historical lake levels and the concurrent seismicity are both subject to significant uncertainties. They stem from the differing nature of the data gathered on these two phenomena and thus deserve special consideration. Earthquake dating can be quite precise, and its accuracy is verified when different historical sources show consensus (Guidoboni et al., 1994; Guidoboni and Comastri, 2005; Ambraseys, 2009). Assessment of the extent of damage (hence earthquake magnitude), similarly requires such a consensus between the different data sources. Sediment records can help to calibrate the analysis of the historical evidence (Agnon, 2014; Kagan et al., 2011). Such records can be tested by trenching (Wechsler et al., 2014; Marco and Klinger, 204; Lefevre, 2018). However, in many cases earthquake epicenter can be

64 imprecise or not even known. Consequently, considerable uncertainty pertains to the historical
65 catalog of earthquakes related directly to the Dead Sea.

66 By contrast, historical water level records are quite precise elevation wise, as they are
67 obtained from different points around the lake (Bookman et al., 2004; Migowski et al., 2006).
68 However, water level dating could have an error of about ±45 yr, as estimated from the radiocarbon
69 dating of shoreline deposits in fan delta outcrops (Bookman et al., 2004). This may underestimate
70 the actual dating uncertainty due to reworking of organic matter, sometimes re-deposited a century
71 or more after equilibration with the atmosphere (Migowski et al., 2004). In addition, the entire past
72 bi-millennial Dead Sea level record is constrained by less than twenty "anchor points" (the data
73 obtained by the dating collected from surveyed paleo-shorelines, Bookman et al., 2004). Therefore,
74 its continuous reconstruction, as suggested in the literature (Migowski et al., 2006; Stern, 2010),
75 usually takes different forms within the acceptable limits dictated by the evidence,
76 geomorphological (Bookman et al., 2004) and limnological (Migowski et al., 2006). A challenging
77 uncertainty for our study arises from the interpolations required for periods when the available
78 data do not constrain the water levels.

79 In this article, we take advantage of the correlation between the historical water level
80 reconstructions at the Dead Sea and seismicity patterns in the area over the past two millennia. We
81 demonstrate for the first time that plausible scenarios for the lake level history can fit very well
82 the record of the historical earthquake recurrence intervals (RIs). Based on the correlation between
83 these phenomena, we offer an alternative explanation regarding the triggering of earthquakes in
84 the area of the Dead Sea.

METHODS

To investigate the relationship between an accurate but discrete chronology of earthquakes and the continuous water level (WL) change, we first explore the space of possible WL histories by a statistical approach. We generate an ensemble of WL curves (based on the anchor points, Bookman et al., 2004), while remaining within the limits dictated by climatic and morphological constraints (Bookman et al., 2004; Migowski et al., 2006; Stern, 2010), by using a random number generator.

In our analysis we associate all the historical earthquakes presented (Table 1A,2A in Appendix) with rupture of the strike-slip faults, which agree with our modeling approach. Hence, the major strike-slip faults constituting the plate boundary (Lower Jordan fault, Dead Sea Lake fault and Northern Arava) could be affected by Dead Sea water level changes. Therefore, our study covers the area within this distance

A best fit random method of WL curve prediction

The compilation of WL curves of the Dead Sea for the last two millennia from three recent publications (Bookman et al., 2004; Migowski et al., 2006 and Stern 2010) is presented in Figure 1A by dashed curves. Generally, the differences between all dashed curves at anchor points is included within an error limit of ±45 yr as indicated by error bars, with an exception of the anchor point dated to 1400 CE (Bookman et al., 2004) for which Migowski et al. (2006) and Stern (2010) suggested a higher WL. Nevertheless, each hypothetical WL curve is forced to pass through all anchor points provided by Bookman et al. (2004) except for one, at around 500 CE. The WL drop around this time, according to Migowski et al. (2006) and Stern (2010), occurred later than was originally suggested by Bookman et al. (2004) (Figure 1A). Because this shift is within the

permissible error limits (±45 yr), this anchor point is shifted to the left (+40 yr). In addition, the WL determined on the curve edges of the studied bi-millennial time interval was defined by additional two anchor points, through which the estimated WL curve passed according to all three references. In total, we have 13 anchor points. Between each pair of points, the trends in the WLs are constrained by the sedimentary facies (Migowski et al., 2006) that specify the edge points of the interval as the extrema for the acceptable WL variation.

However, within the largest interval between the anchor points (600 - 1100 CE), the field studies (Migowski et al., 2006; Stern, 2010; Bookman et al., 2004) constrained the WL to be lower than the extrema at the edges of that interval. For this period, the WL was randomly interpolated between the higher (e.g., Migowski et al., 2006) and lower (e.g., Stern, 2010) bounds. To maintain a monotony of the WL variation (required by the facies analysis of Migowski et al.), a moving average filtered the random noise between every pair of the anchor points. Accounting for the above-mentioned limits, and setting a ten-year step, the model has generated 10 million WL curves for the last bimillennial interval, using a uniformly distributed random number generator.

We test for linear correlation between the recurrence intervals (RIs) of the widely recorded moderate-to-large (M>5.5) historical earthquakes available from the literature (Table 1 and the text description in Appendix), and the WL interpolations (as in Figure 9 in Belferman et al., 2018); and evaluate the values of the Pearson product-moment correlation coefficient, R (Figure 1B). We use this statistic for evaluating the suitability of each randomly interpolated WL curve for our analysis, for identification and elimination of any outliers, and for studying the behavior of the entire ensemble of the curves generated.

The earthquake simulation algorithm

The most suitable WL curve suggested by this correlation (discussed in the results section below), was used to generate a "synthetic" earthquake catalog based on the algorithm described in this section. Effective (normal) poroelastic stress change due to the WL change is superimposed on the tectonic stress accumulated consistently with the slip rate since the preceding seismic event, and synthetic earthquakes are simulated using a Coulomb failure envelope and a Mohr circle (e.g. Jaeger et al., 2009). A vertical strike-slip fault below the lake/reservoir bed is assumed (simulating a Dead Sea fault), embedded in the 2D (plain strain) geometry of the upper crust (Belferman et al., 2018). Tectonic horizontal strike-slip displacements across the fault are approximated by a simple shear approach with no normal strain component.

In the poroelastic part of the model, horizontal stress change normal to the strike slip fault produced by the water level change, is calculated under a uniaxial (vertical) strain condition (Eq.10b in Belferman et al., 2018). This is applicable to a post-diffusion stage: i.e., when pore pressure at hypocentral depth equilibrates with the lake's bed. An array of the effective horizontal normal stress changes, $\Delta\sigma_i'$, at the fault, induced by the water load change at the lake's bed, p_{s_i}, corresponds to the array of the WL change, $\Delta h_i (i = 1,2, \dots 2000)$ over the interpolated water level curve, Figure 1D:

1. $$\Delta\sigma_i' = \frac{1-2\nu}{1-\nu}(\beta - 1)p_{s_i}$$

(Eq. 10b in Belferman et al., 2018). Here β is Biot's coefficient and ν is the Poisson's ratio, $p_{s_i} = \rho g \Delta h_i$, where ρ is the density of water and g is the acceleration of gravity.

A radius and a center location of the Mohr circle change as a function of the tectonic deformations and water level changes, correspondingly, eventually reaching a failure envelope that simulates an earthquake. The model uses a Byerlee's law envelope (Byerlee, 1978) to define

a residual strength of a seismogenic zone at the fault immediately after the earthquake (Belferman et al., 2018 for more detail). Since the effective stress upon the onset of an earthquake is specified by a high failure envelope and the effective stress following the slip is given by Byerlee's law (e.g., Belferman et al., 2018), the model is time-predictable. The stress drop, at least in the nucleation zone of a single-fault model, is expected to be proportional to the recurrence interval.

A starting point of the simulations is the date of the first historical earthquake (33CE, Table 1 in the Appendix) from the bi-millennial time interval studied. The simulation incrementally proceeds with time over the WL curve generated (as above) under the accumulating tectonic stress. After each stress release, the time to the next earthquake, Δt, is calculated from the solution of the Mohr-Coulomb failure criterion for a strike-slip tectonic regime and a WL change, Δh_i, characteristic of the Dead Sea fault (Belferman, et al., 2018):

$$(\tau_i - \tau_0)^2 + \left(\sigma_i - (\sigma_0 + \Delta\sigma_i')\right)^2 = \left(R_0 + \Delta\tau_{xy_i}\right)^2 \quad (2.)$$

$$\tau_i = C + tan(\varphi)\sigma_i$$

assuming that $\Delta\tau_{xy_i} = \frac{Ccos(\varphi)}{t_{RI}}\Delta t$ is the tectonic shear stress accumulated consistently with slip-rate at the strike-slip fault during the period Δt (time passed since the last earthquake), C is cohesion, φ is an angle of internal friction, σ_0 and τ_0 are the coordinates of the Mohr circle center immediately after the earthquake and R_0 its radius, t_{RI} is the reference RI corresponding to the minimal WL.

For each time step, the algorithm determines whether there is a single solution, or two, or nil. A case of no solutions means that the Mohr circle is yet to reach the failure envelope, as the accumulating tectonic stress and the WL increase are still insufficient. The system of Eq. 2 may

have a single solution when the failure criterion is met at the end of some timestep, or two solutions when it is met before the end of the timestep. A case of two solutions is rounded down to a case of a single solution if a time step (one year) is small compared to the earthquake RI (several hundreds of years).

This solution of Eq.2 yields a RI as a function of the effective normal horizontal stress change, $\Delta\sigma_i'$ (Belferman et al., 2018):

$$RI = \Delta t = (C + tan(\varphi)\Delta\sigma_i')\frac{t_{RI}}{C} \quad (3.)$$

where t_{RI} is the reference RI corresponding to the minimal WL, C is cohesion, φ is an angle of internal friction. From this formula, an array of earthquake dates is obtained.

Substitution of Eq.1 into Eq.3, yields a linear dependence of a simulated *RI* on a WL change, Δh_i, evolving with time.

$$RI = t_{RI} + \frac{tan(\varphi)}{C}\frac{1-2\nu}{1-\nu}(\beta - 1)\rho g t_{RI}\Delta h_i \quad (4.)$$

A tectonic slip-rate is set at 5 mm/yr (e.g. Hamiel et al., 2018; Hamiel and Piatibratova, 2019; Masson et al., 2015). Coefficients for the simulations were previously determined in Belferman et al. (2018). Note that the cohesion, C, is not a-priory known, hence it is fixed by the empirical correlation between WL and RI for a given lake level history considered. Its value, $C = 0.08Mpa$, and a reference RI, $t_{RI} = 300yr$, were adjusted numerically for a WL curve, providing the average RI of 144 yr over the modeled period of two millennia justified by historical, archaeological, and geological data (Agnon, 2014).

RESULTS

Ten most suitable WL curves are identified out of the 10M set of WL randomly generated curves ("ensemble") by the Pearson product-moment correlation test. The values of the correlation coefficients, R, for the entire ensemble are distributed normally around R=0.63 (Figure 1B) with a standard deviation of σ =0.076. The ten most suitable WL curves ordered by their correlation coefficients, R, are presented in Figure 2.

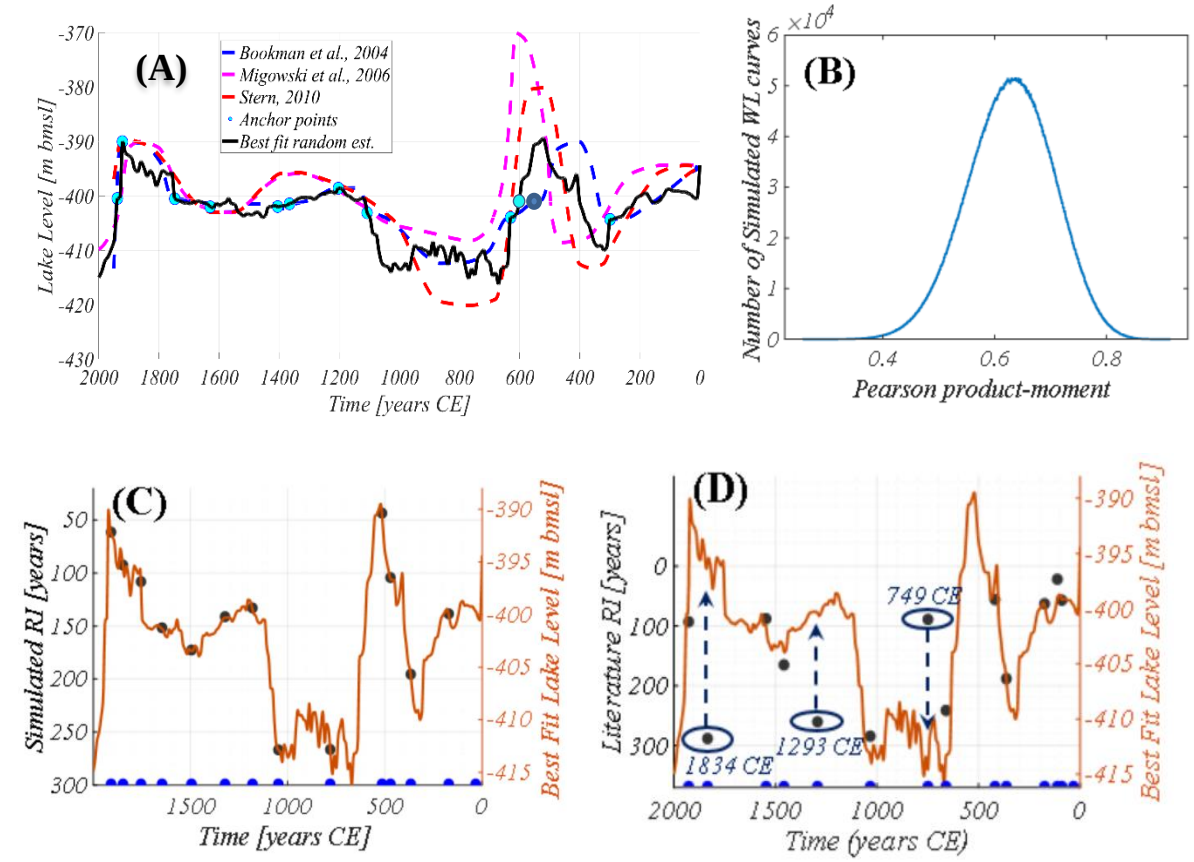

Figure 1: ***(A)*** *The Dead Sea WL reconstructions for the last two millennia. The dashed curves are suggested by the literature sources. Turquoise anchor points follow Bookman et al. (2004) used in WL interpretation, while one point (in dark blue) is shifted to left in error interval of* $\pm$ *45 yr. Solid, black line water curve is suggested by this study.* ***(B)*** *Distribution of Pearson's product-moment correlation coefficient of randomly interpolated WLs and RIs of historic earthquakes. Normal distribution results from 10M random WLs reconstructions.* ***(C)*** *and* ***(D):*** *Orange curve represents the best fit random WL curve vs. simulated and historic RIs, correspondingly. The blue dots mark the dates of the seismic events, while the black dots indicate the recurrence interval between these events. For optimal visualization of the correlation, the degree of scaling freedom for the RI axis was set for these figures.* ***(E)*** *Dates of historic vs. simulated earthquakes based on the suggested best fit WLs curve (Figs.C,D), are compared.*

197

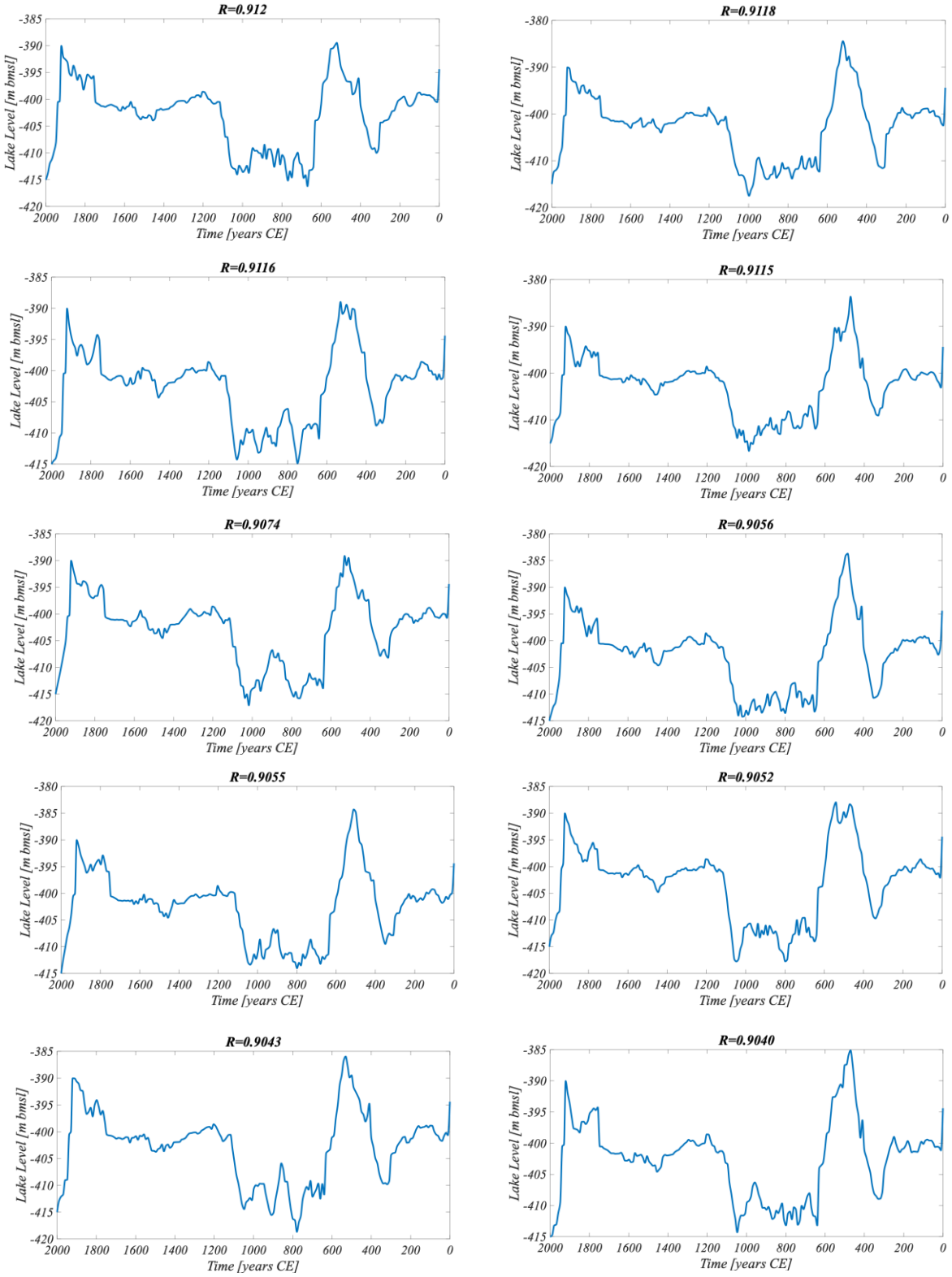

Figure 2: *Ten most suitable WLs identified out of the 10M randomly generated by the Pearson product-moment correlation test.*

198

Three outliers from the thirteen RIs of the widely recorded historic earthquakes (749 CE, 1293 CE and 1834 CE in Figure 1) were identified and reevaluated (explanation in Appendix). A curve with the highest Pearson coefficient of R=0.912 was chosen from the correlation between the RIs of the revised historic catalog and the randomly generated WLs (Figure 2). This correlation can be specified by a linear prediction function:

$$RI = -5442 - 14WL \quad (5.)$$

where RI is given in years and WL in meters. In addition, a synthetic earthquake history including 14 seismic events was simulated from the best fit randomly interpolated WL curve with R=1 specified above. The synthetic RIs can be approximated based on the WLs using the linear relationship Eq.4):

$$RI = -3840 - 10WL \quad (6.)$$

The dates of the simulated synthetic earthquakes are presented, versus the dates of the historical earthquakes from the literature (Table A1, Appendix) in Figure 1E.

The synthetic earthquake stress history is presented in Figure 3. The effective horizontal normal stress change, $\Delta\sigma_i'$, (Figure 3A) linearly depends on the water level (Eq.1.), and as expected, follows its variability. The tectonic shear stress change, $\Delta\tau_{xy}$, drops to zero after the accumulated shear stress is released by the strike-slip earthquake (Figure 3B). Less shear stress is required to induce the earthquake when the change in water level is larger (Figures 3A,3B), modeled with Mohr-Coulomb failure criteria (Figure 3C) (explained also in Belferman et. al., 2018).

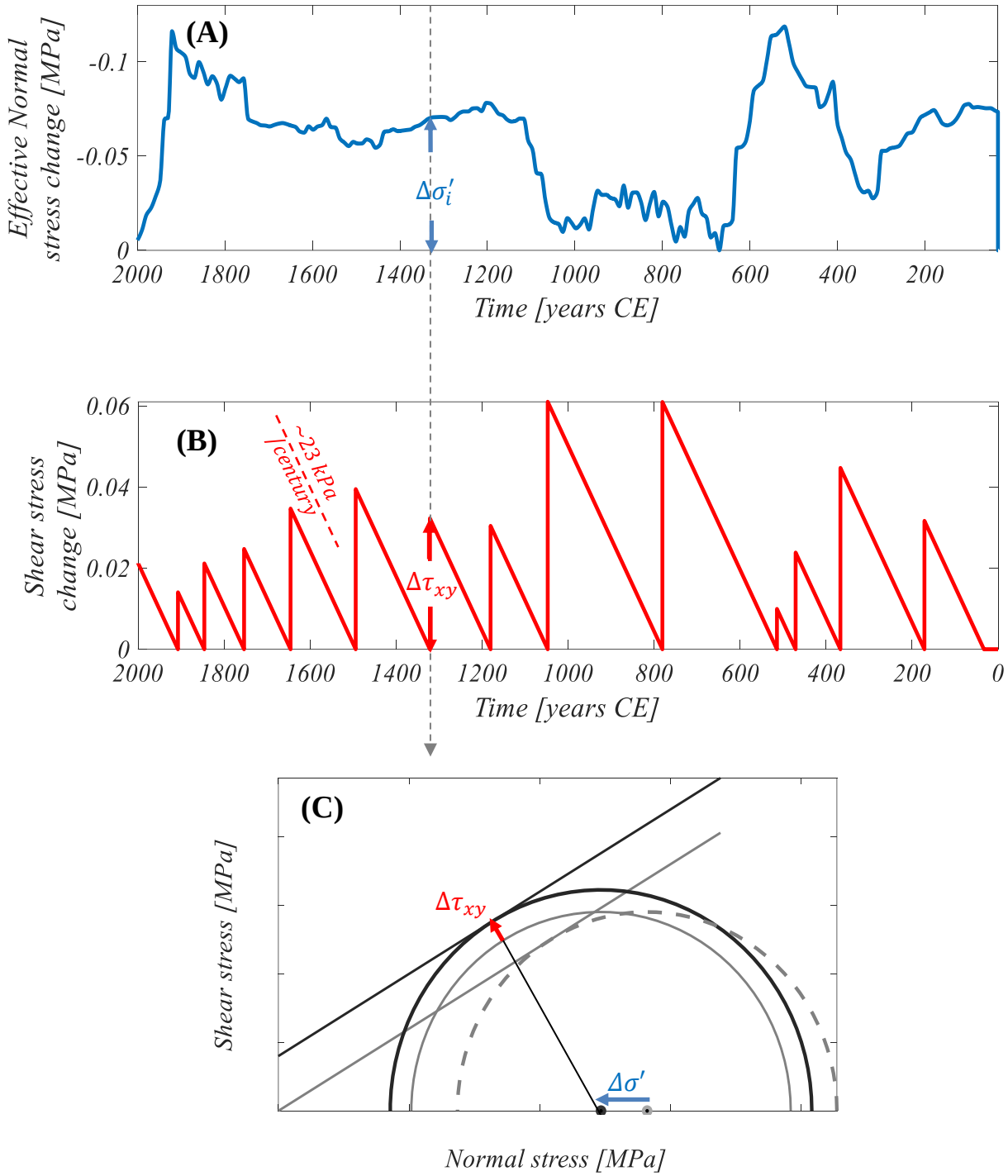

Figure 3: ***(A)*** *The effective normal stress change, $\Delta\sigma'$, induced by water level change, Eq.1.* ***(B)****Tectonic shear stress change, $\Delta\tau_{xy}$, accumulated consistently with slip-rate on the strike-slip fault during the time passed since the last earthquake. The shear stress accumulation rate, used in this study is about 23 kPa/century (formulation below Eq. 2, following Belferman et al., 2018)* ***(C)*** *Evolution of the stress change on the fault due to combined tectonic and water loading. The state of the effective stress at the fault immediately after an earthquake is restricted by the Byerlee's law envelope with zero cohesion, C=0, and a friction angle, $\varphi = 0.54^o$. The center of the Mohr circle is located at (σ_0,τ_0=0 see Belferman et al., 2018 for more detail). The failure envelope is defined by C≥0 and $\varphi = 0.54^o$. The left shift in the center of the circle by $\Delta\sigma'$ represents pore pressure (due to water level) change at this moment (Fig.3A); the increase in radius represents tectonic shear stress, $\Delta\tau_{xy}$, accumulated during the inter-seismic period (Fig.3B). Failure occurs when the circle tangents the failure envelope (presented here for the representatve 1320 CE earthquake).*

DISCUSSION

Uncertainties in the WL reconstructions associated with dating and resolution lead to considerable variance in possible interpolations (Figure 1B). A Pearson correlation coefficient test shows that most of the randomly interpolated WL curves give linear correlation with earthquake RIs (indicated by a mean Pearson coefficient of R=0.63), excluding the three outliers (Figure 1D) to be discussed below. Figure 2 shows a similar pattern of the WL change for the ten most correlated curves. In all cases, a significant rise in the water level of about 400 CE and 1100 CE is visible and a decrease in the WL around 200 and 600 CE. Also, the maximum level around 500 and 1900 CE appears in all ten cases.

For simulating synthetic earthquakes triggered by the WL change, we use the WL curve that generates the highest correlation with the revised historical catalog (R = 0.912) (Figure 2). The dates of these simulated synthetic earthquakes are comparable with historical earthquakes (Figure 1E) excluding two events, whose date labels are offset to the y-axis for clarity of presentation (1753 CE, 1180 CE). The dates of these synthetic earthquakes might be connected to three outliers from the historical catalog (1834 CE, 1293 CE and 749 CE depicted in Figure 1D) as explained below.

The 1180 CE synthetic earthquake (Figure 1E) is comparable to an earthquake in the literature dated by Ben-Menachem (1979) and Amiran et al. (1994) to the mid-12th century (~1150 CE). Ambraseys (2009) doubted the precise dating but accepted this mid-12th century estimate. The damaged area of this earthquake spanned Jericho and Jerusalem, and the event could be considered significant because it led to the total destruction of two monasteries, one of which is 10 km south of Jerusalem's curtain wall. By admitting the ~1150 CE earthquake to the amended

242 catalog, we reduce the RI of the subsequent earthquake at 1293 CE (Figure 1D) from 260 to 143
243 yrs, thereby bringing this outlier very close to the linear correlation.

244 Our model also generates an earthquake in the 18th century, dated 1753 CE, for which there
245 were no matches in our initial historical catalog (Belferman et al., 2018). However, in Amiran's et
246 al. (1994) catalog an earthquake in 1712 CE is indicated: 'The quake shook the solid houses and
247 ruined three Turkish houses. Felt in Ramle, but not in Jaffa'. Additionally, this earthquake is
248 evidenced by seismites dated to 1700 – 1712 CE from an Ein Gedi site (Migowski et al., 2004).

249 Regarding the modeled 1907 CE event, we note the well-documented (although often
250 overlooked) 29 March 1903 CE earthquake (Amiran et al., 1994). This was a moderate but
251 prolonged earthquake: local intensity reached VII in a number of localities distributed outside the
252 rift valley over an area of 140x70 square km (including Jerusalem), whereas the maximum
253 intensity reported in the rift was VII as well (Jericho). We prefer to correlate the modeled 1907
254 event with the stronger 1927 Jericho earthquake that clearly released stress in the Dead Sea (e.g.
255 Shapira, et al., 1993; Avni et al., 2002; Agnon, 2014). This leaves the 1903 CE unmatched to our
256 model. Perhaps the earthquake ruptured the northern part of the central Jordan Valley, north of the
257 Dead Sea and south of Lake Kinneret (Sea of Galilee).

258 Regarding the last outlier from the historical earthquakes dated to 749 CE (or its neighbors
259 747 and 757, Table A1 in the Appendix) (Figure 1D) and corresponding to the simulated 780 CE
260 earthquake (Figure 1E): the simulation generated the preceding earthquake 514 CE associated with
261 the 659/660 CE event from the literature (Table A1 in the Appendix) with a deviation of 146 years.
262 The rupture zone of the 659/660 CE event is uncertain, and this earthquake is not necessarily
263 related to stress-release at the Dead Sea basin. Alternatively, following Russell (1985), as a result

of the 551 CE earthquake, a fortress east of the southern Dead Sea and Petra were destroyed. Newer data contradicts the assertion regarding Petra; a failure in the Dead Sea region is still plausible. Replacing the 660 CE earthquake with 551 CE in the catalog changes the RI preceding the 749 CE historical earthquake from 89 to 198, which brings this outlier into a satisfactory linear correlation (Figure 1D).

Additionally, it should be emphasized that in the simulation presented in this article, the starting point is quite arbitrarily, the earthquake of 33 CE. This event together with the subsequent earthquakes 90 CE and 112 CE (not predicted by our model) span a single century where the catalog is nebulous. Each of these events could thus represent the starting point of the simulations or could be omitted at this early and poorly documented interval.

Summarizing the above amendments, we add to our catalog of historical events the 551 CE, ~1150 CE and 1712 CE earthquakes, and remove 559/660 CE and 90 CE, 112 CE earthquakes (Figure 1E). Altogether, we get 14 triggered historical earthquakes. The correlation between the water level and recurrence interval is noticeable for the various variants of the water level curve reconstruction (Figure 4).

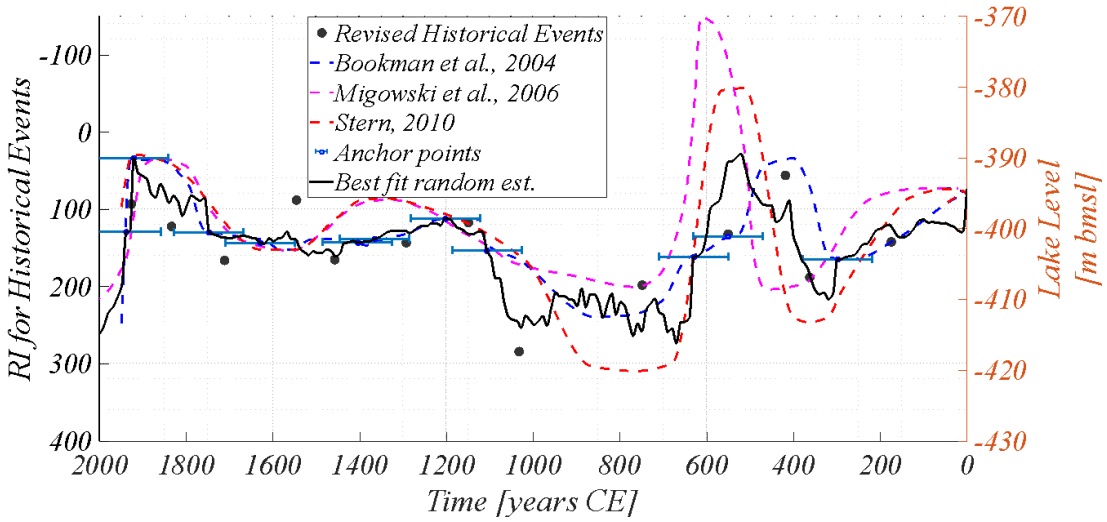

Figure 4: *The Dead Sea WL reconstruction for the last two millennia. The dashed curves are suggested by the literature. Blue anchor points with an error interval of ±45 yr. follow Bookman et al. (2004). The solid black line is the water level curve suggested by this study. The black points represent the RI for revised historical events, suggested in this study as being relevant to the Dead Sea area.*

The correlation of RI with the best fit random estimated curve can be specified by a linear prediction function:

$$RI = -2483 - 6.5WL \quad (7.)$$

This linear relationship between WL and RI underscores the previously proposed correlations between these phenomena (in Figure 9 in Belferman et al., 2018).

Since the last earthquake (1927 CE), the water level in the Dead Sea has continuously decreased at an average annual rate of ~1 m/yr. Today the water level is about -440 (m bmsl), thus our prediction function (Eq. 7) suggests a RI of 377 yr, for such a WL. Namely, should the water level in the Dead Sea remain constant (-440 m bmsl), as intended in some mitigation plans, we would expect the next earthquake at about ~2300 CE.

This paper stresses that reconstruction of WL curves is not unique and may take various forms under the constraints available (e.g., Figure 1A). However, the correlation with an

independent record of RIs of seismic events, assuming that earthquakes are affected by WL hikes, allows deciphering plausible scenarios for WL evolution. Moreover, for cases with the best but not perfect correlation, the deviation might be consistent with a release of elastic energy by smaller earthquakes, which are not accounted for by the deterministic part of our model. We note that smaller earthquakes might rupture dip-slip fault planes, again not accounted for by our simple model.

Additionally, as large earthquakes are accompanied by aftershocks, some of the elastic energy is released by them. It was shown earlier that in areas of reservoir-induced seismicity, earthquakes are not only accompanied by aftershocks but also preceded by foreshocks (Gupta, 2011). The decay curve of this kind of seismicity satisfies the criteria for the second class of earthquake sequences by Mogi (1963). The lack of instrumental records of historical earthquakes in our study area does not allow comparison with this class. The 1995 Gulf of Aqaba earthquake (7.2 Mw), the last large instrumentally recorded earthquake, was accompanied by a long period (significant enough for stress release consideration) of the aftershocks. The earthquake occurred along the southern part of the plate boundary, which is far enough from the Dead Sea, and most likely is not influenced by the water level change. Following this earthquake felt aftershocks continued for about two years. At least 50 percent of the total moment associated with these aftershocks was released during the first day after the main shock and over 95 percent in the first 3 months (Baer, 2008). In total, the post-seismic moment released during the period of 6 months to 2 yr after the Nuweiba earthquake is about 15 percent of the co-seismic moment release (Baer, 2008). This earthquake showed that the response of the crust to earthquakes by aftershocks is negligible, as noted for many large earthquakes (e.g., Scholz, 1972).

For the case of artificial reservoirs, it was shown that for reservoir-induced seismicity sequences, aftershocks continue for a longer time than for tectonic earthquake sequences (Gupta, 2011). However, given the time scale of RI, the period of aftershocks is insufficient to consider earthquakes from the sequence in our model as separate events. Regarding the time scale presented in our study, when the minimal inter-seismic period is about 50 years, the stress released during a post-seismic period can be considered a part of the main shock.

The mechanical model used in this article is rather simplistic, where earthquakes release the strike-slip component of the tectonic loading (Figure 3B). The basins around the Dead Sea fault system also testify for an extensional component that could be manifested in co-seismic motion along normal faults. To justify our focus on a single type of fault (strike-slip), we list the following arguments:

- The far-field maximal and minimal principal stresses in the Dead Sea region are horizontal (Hofstetter et al., 2007; Palano et al. 2013). This is compatible with the dominance of strike-slip faulting (Anderson, 1951). The tectonic motion at the DSF is characterized predominantly by a left-lateral strike-slip regime with a velocity of ~5 mm/yr along various segments (Garfunkel, 2014; Masson et al.,2015; Sadeh et al., 2012). Large earthquakes that initiate clusters are likely to rupture along the straight ~100 km strike-slip segments (Lyakhovsky et al., 2001). The strike of these segments parallels the relative plate velocity vector and thus can be approximated by simple shear. Additionally, in the Dead Sea basin, GPS surveys indicate the dominance of strike-slip loading. Hamiel et al. (2018) show that, on a plate scale, horizontal shear loading dominates the velocity north of the lake. Hamiel and Piatibratova (2019) detected a sub-mm/yr component of extension across the southern

normal fault bounding the Dead Sea pull-apart (Amatzyahu Fault); yet the strike-slip component across this very fault is much larger.

- Normal, as well as strike-slip faults, similarly react to water level change that contributes to the vertical stress component and pore pressure change. The seismicity induced by surface water level fluctuations and affected by the faulting regime is critically determined by the relative orientations of the three principal stresses in the Earth's crust (Anderson, 1951). In regions where the vertical compressive stress is not minimal (normal and strike-slip faulting), seismic activity is more sensitive to the effective stress change due to water level change, than in regions where it is minimal (thrust faulting) (Simpson, 1976; Snow, 1982; Roeloffs, 1988). This is applicable to reservoirs approximated as "infinite" in the horizontal plane (e.g., Wang, 2000), with respect to the fault zone horizontal cross-section. Since we are using a one-dimensional model, such approximation is valid for our study area where the Dead Sea is large enough in a horizontal plane (100 km x 10 km) compared to the thickness of the underlying strike-slip fault (cross-section) located in the central part of the valley.

Our results demonstrate that a fairly simple forward model (based on 1D analytical solution, Belferman et al., 2018) achieves a convincing correlation between WLs and RIs of moderate-to-strong earthquakes on the Dead Sea fault. Whereas the fault system along the Dead Sea fault is more complicated, three-dimensional modeling of the tectonic motion, coupled with the pore pressure evolution, may give more reliable predictions regarding earthquake ruptures and their chronology. However, based on the relationship between the WL and RI changes presented in this article, with the current anthropogenic decrease in the Dead Sea level (with an average annual rate of ~ 1 m / yr), a moderate to severe earthquake will not be triggered by the mechanism

discussed here. This article not only suggests the existence of a connection between WL and RI, but also provides additional guidance based on this connection.

DATA AVAILABILITY

All raw data can be provided by the corresponding authors upon request.

AUTHOR CONTRIBUTIONS

MB and AA Conceptualization; AA data collection and analysis; MB Modelling, data visualization and results analysis; RK Validation; MB original draft preparation; MB, RK and AA review and revisions; AA, ZB and RK Funding acquisition and Resources.

COMPETING INTERESTS

The authors declare that they have no conflict of interest.

ACKNOWLEDGMENTS

This project was supported by grants from the Ministry of Natural Infrastructures, Energy and Water Resources of Israel # *213-17-002*, GIF- German - Israeli Foundation for Scientific Research and Development # I-1280-301.8, and by PhD fellowships from the University of Haifa, Israel. The data for this paper were obtained with analytical and numerical modeling.

REFERENCE

Agnon A. 2014. Pre-instrumental earthquakes along the Dead Sea rift. In Dead Sea transform fault system: reviews, edited by Garfunkel, Zvi, Ben-Avraham, Zvi, Kagan, Elisa, 207-261, Springer, Dordrecht. ***https://doi.org/10.1007/978-94-017-8872-4_8***.

Ambraseys, N. 2009. Earthquakes in the Mediterranean and Middle East: a multidisciplinary study of seismicity up to 1900. Cambridge University Press. doi: ***https://doi.org/10.1017/CBO9781139195430***

385 Ambraseys, N. N., Melville, C. P. and Adams, R. D. *1994.* The Seismicity of Egypt, Arabia and
386 the Red Se: A Historical Review. Cambridge: Cambridge Univ. Press.
387 ***https://doi.org/10.1017/S1356186300007240***

388 Amiran, D. H., Arieh, E., and Turcotte, T. 1994. Earthquakes in Israel and adjacent areas:
389 macroscopic observations since 100 B.C.E. *Israel Exploration Journal, 44*, 260– 305.
390 ***http://www.jstor.org/stable/27926357.***

391 Anderson, E. M. (1951). The dynamics of faulting and dyke formation with applications to Britain.
392 Oliver and Boyd.Avni, R., Bowman, D., Shapira, A. and Nur, A. 2002. Erroneous
393 interpretation of historical documents related to the epicenter of the 1927 Jericho
394 earthquake in the Holy Land. *Journal of seismology*, 6(4), 469-476.
395 ***https://doi.org/10.1023/A:1021191824396***

396 Baer G., G. J. Funning, G. Shamir, T. J. Wright (2008). The 1995 November 22, Mw 7.2 Gulf of
397 Elat earthquake cycle revisited, Geophysical Journal International, 175(3), 1040-
398 1054. ***https://doi.org/10.1111/j.1365-246X.2008.03901.x***

399 Belferman, M., Katsman, R. and Agnon, A. 2018. Effect of large-scale surface water level
400 fluctuations on earthquake recurrence interval under strike-slip faulting. *Tectonophysics*,
401 744, 390-402. ***https://doi.org/10.1016/j.tecto.2018.06.004***

402 Ben-Menahem, A. 1979. Earthquake catalogue for the Middle East (92 BC-1980 AD). *Boll.*
403 *Geofis. Teor. Appl.*, 21, 245-313.

404 Bookman, R., Enzel, Y., Agnon, A., and Stein, M. 2004. Late Holocene lake levels of the Dead
405 Sea. *Geological Society of America Bulletin* 116, 555-571. ***https://doi.org/10.1130/B25286.1***

406 Byerlee, J.D., 1978. Friction of rocks. In: Byerlee, J.D., Wyss, M. (Eds.), Rock Friction and
407 Earthquake Prediction. *Springer, Birkhäuser, Basel*, pp. 615–626.
408 ***https://doi.org/10.1007/978-3-0348-7182-2***

409 Durá-Gómez, I. and Talwani, P. 2010. Reservoir-induced seismicity associated with the Itoiz
410 Reservoir, Spain: a case study, *Geophysical Journal International*, 181, 343–356.
411 ***https://doi.org/10.1111/j.1365-246X.2009.04462.x***

412 Elad, A. 1982. An early Arabic source concerning the markets of Jerusalem. *Cathedra*, 24, 31-40.

413 Elad, A., 1992. Two Identical Inscriptions From Jund Filastin From the Reign of the Abbāsid
414 Caliph, Al-Muqtadir. *Journal of the Economic and Social History of the Orient*, *35*(4),
415 301-360. ***https://doi.org/10.2307/3632739***

416 Garfunkel, Z., 2014. Lateral motion and deformation along the Dead Sea Transform. In: Garfunkel,
417 Z., Ben-Avraham, Z., Kagan, E. (Eds.), Dead Sea Transform Fault System: Reviews. 5.
418 Springer, Dordrecht, pp. 109–150. ***http://dx.doi.org/10.1007/978-94-017-8872-4.***

419 Gerber, H., 1998. " Palestine" and Other Territorial Concepts in the 17th Century. *International*
420 *Journal of Middle East Studies*, 30(4), 563-572. ***https://www.jstor.org/stable/164341***

421 Guidoboni, E., Comastri, A., and Traina, G. 1994. Catalogue of Ancient Earthquakes in the
422 Mediterranean Area Up to the 10th Century. Rome: Istituto nazionale di geofisica.
423 ***https://doi.org/10.1163/182539185X01377***

424 Guidoboni, E. and Comastri, A. 2005. Catalogue of Earthquakes and Tsunamis in the
425 Mediterranean Area from the 11th to the 15th Century. Istituto nazionale di geofisica e
426 vulcanologia. ***https://doi.org/10.1515/BYZS.2008.854***

Gupta, H., K., 2018, Reservoir triggered seismicity (RTS) at Koyna, India, over the past 50 yrs. *Bulletin of the Seismological Society of America* 108.5B: 2907-2918. ***https://doi.org/10.1785/0120180019***

Hamiel, Y., Masson, F., Piatibratova, O., & Mizrahi, Y. (2018). GPS measurements of crustal deformation across the southern Arava Valley section of the Dead Sea Fault and implications to regional seismic hazard assessment. Tectonophysics, 724, 171-178. ***https://doi.org/10.1016/j.tecto.2018.01.016***

Hamiel, Y., & Piatibratova, O. (2019). Style and distribution of slip at the margin of a pull-apart structure: Geodetic investigation of the Southern Dead Sea Basin. Journal of Geophysical Research: Solid Earth, 124(11), 12023-12033. ***https://doi.org/10.1029/2019JB018456***

Hofstetter, R., Klinger, Y., Amrat, A. Q., Rivera, L., & Dorbath, L. (2007). Stress tensor and focal mechanisms along the Dead Sea fault and related structural elements based on seismological data. Tectonophysics, 429(3-4), 165-181. ***https://doi.org/10.1016/j.tecto.2006.03.010***

Hua, W., Chen, Z. and Zheng, S., 2013a. Source parameters and scaling relations for reservoir induced seismicity in the Longtan reservoir area. Pure Appl. Geophys. 170, 767–783. ***https://doi.org/10.1007/s00024-012-0459-7***

Hua, W., Chen, Z., Zheng, S., and Yan, C., 2013b. Reservoir-induced seismicity in the Longtan reservoir, southwestern China. J. Seismol. 17 (2), 667–681. ***https://doi.org/10.1007/s10950-012-9345-0***

Hough S. E. and Avni R., 2011. The 1170 and 1202 CE Dead Sea Rift earthquakes and long-term magnitude distribution of the Dead Sea Fault Zone, *Isr. J. Earth Sci.*, 58, 295–308. ***ttps://doi.org/10.1560/IJES.58.3-4.295***

Jaeger, J. C., Cook, N. G., & Zimmerman, R. (2009). Fundamentals of rock mechanics. John Wiley and Sons.

Kagan, E., Stein, M., Agnon, A., and Neumann, F. 2011. Intrabasin paleoearthquake and quiescence correlation of the late Holocene Dead Sea. Journal of Geophysical Research*: Solid Earth*, 116(B4). ***https://doi.org/10.1029/2010JB007452***

Ken-Tor, R., Agnon, A., Enzel, Y., Stein, M., Marco, S., and Negendank, J. F. 2001. High-resolution geological record of historic earthquakes in the Dead Sea basin. *Journal of Geophysical Research-Solid Earth, 106*, 2221-2234. ***https://doi.org/10.1029/2000JB900313***

Langgut, D., Yannai, E., Taxel, I., Agnon, A. and Marco, S., 2015. Resolving a historical earthquake date at Tel Yavneh (central Israel) using pollen seasonality. *Palynology*, *40(2)*, 145-159. ***https://doi.org/10.1080/01916122.2015.1035405***

Lefevre, M., Klinger, Y., Al-Qaryouti, M., Le Béon, M. and Moumani, K., 2018. Slip deficit and temporal clustering along the Dead Sea fault from paleoseismological investigations. Sci. Rep. 8 (1), 4511. ***https://doi.org/10.1038/s41598-018-22627-9***

Lyakhovsky, V., Ben-Zion, Y., Agnon, A., 2001. Earthquake cycle, fault zones, and seismicity patterns in a rheologically layered lithosphere. J. Geophys. Res. Solid Earth 106 (B3), 4103–4120.

468 Marco, S., Stein, M., Agnon, A., and Ron, H. 1996. Long-term earthquake clustering: A 50,000-
469 year paleoseismic record in the Dead Sea Graben. Journal of Geophysical Research: Solid
470 Earth, 101(B3), 6179-6191. ***https://doi.org/10.1029/95JB01587***

471 Masson, F., Hamiel, Y., Agnon, A., Klinger, Y. and Deprez, A., 2015. Variable behavior of the
472 Dead Sea Fault along the southern Arava segment from GPS measurements. comptes
473 rendus geoscience, 347(4), pp.161-169. ***https://doi.org/10.1016/j.crte.2014.11.001***

474 Migowski, C., Agnon, A., Bookman, R., Negendank, J. F., and Stein, M. 2004. Recurrence pattern
475 of Holocene earthquakes along the Dead Sea transform revealed by varve-counting and
476 radiocarbon dating of lacustrine sediments. *Earth and Planetary Science Letters*, *222*, 301–
477 314. ***https://doi.org/10.1016/j.epsl.2004.02.015***

478 Migowski, C., Stein, M., Prasad, S., Negendank, J. F. W., and Agnon, A. 2006. Holocene climate
479 variability and cultural evolution in the Near East from the Dead Sea sedimentary record.
480 *Quaternary Research*, 66(3), 421-431. ***https://doi.org/10.1016/j.yqres.2006.06.010***

481 Palano, M., Imprescia, P., & Gresta, S. (2013). Current stress and strain-rate fields across the Dead
482 Sea Fault System: Constraints from seismological data and GPS observations. Earth and
483 Planetary Science Letters, 369, 305-316. ***https://doi.org/10.1016/j.epsl.2013.03.043***

484 Pandey, A.P. and Chadha, R.K., 2003. Surface loading and triggered earthquakes in the Koyna–
485 Warna region, western India. *Phys. Earth Planet. Inter.* 139 (3–4), 207–223.
486 ***http://dx.doi.org/10.1016/j.pepi.2003.08.003***

487 Parker, S.T., 1982. Preliminary Report on the 1980 Season of the Central" Limes Arabicus"
488 Project. *Bulletin of the American Schools of Oriental Research*, *247*(1), pp.1-26.
489 ***https://www.journals.uchicago.edu/doi/10.2307/1356476***

Rao, N. P., & Shashidhar, D. (2016). Periodic variation of stress field in the Koyna–Warna reservoir triggered seismic zone inferred from focal mechanism studies. Tectonophysics, 679, 29-40. ***https://doi.org/10.1016/j.tecto.2016.04.036***

Russell, K. W., 1985. The earthquake chronology of Palestine and northwest Arabia from the 2nd through the mid-8th century AD. Bulletin of the American Schools of Oriental Research, 260(1), 37-59. ***https://doi.org/10.2307/1356863***

Sadeh, M., Hamiel, Y., Ziv, A., Bock, Y., Fang, P., Wdowinski, S., 2012. Crustal deformation along the Dead Sea Transform and the Carmel Fault inferred from 12 years of GPS measurements. J. Geophys. Res. Solid Earth 117, B08410. ***http://dx.doi.org/10.1029/2012JB009241.***

Scholz, C. H. (1972). Crustal movements in tectonic areas. Tectonophysics, 14(3-4), 201-217. ***https://doi.org/10.1016/0040-1951(72)90069-8***

Shapira, A., Avni, R., and Nur, A. 1993. A new estimate for the epicenter of the Jericho earthquake of 11 July 1927. *Isr. J. Earth Sci,* 42(2), 93-96.

Simpson, D. W. (1976). Seismicity changes associated with reservoir loading. Engineering Geology, 10(2-4), 123-150. ***https://doi.org/10.1016/0013-7952(76)90016-8***

Simpson, D. W., Leith, W., and Scholz, C. 1988. Two types of reservoir-induced seismicity. *Bulletin of the Seismological Society of America, 78*, 2025–2040.

Snow, D. T. (1982). Hydrogeology of induced seismicity and tectonism: Case histories of Kariba and Koyna. Geological Society of America Special Papers, 189, 317-360. ***https://doi.org/10.1130/SPE189-p317***

Stern, O. 2010. Geochemistry, Hydrology and Paleo-Hydrology of Ein Qedem Spring System; Report GSI/17/2010; Geological Survey of Israel: Jerusalem, Israel, 2010; p. 91. (In Hebrew)

Talwani, P., 1997. On the nature of reservoir-induced seismicity. Pure Appl. Geophys. 150, 473–492. ***https://doi.org/10.1007/978-3-0348-8814-1_8***

Wang, H., 2000. Theory of Linear Poroelasticity With Applications to Geomechanics and Hydrogeology. University Press, Princeton.

Wechsler, N., Rockwell, T. K., Klinger, Y., Štěpančíková, P., Kanari, M., Marco, S., & Agnon, A. (2014). A paleoseismic record of earthquakes for the Dead Sea transform fault between the first and seventh centuries CE: Nonperiodic behavior of a plate boundary fault. *Bulletin of the Seismological Society of America*, 104(3), 1329-1347. ***https://doi.org/10.1785/0120130304***

Williams, J. B., Schwab, M. J., & Brauer, A. 2012. An early first-century earthquake in the Dead Sea. *International Geology Review*, *54*(10), 1219-1228. ***https://doi.org/10.1080/00206814.2011.639996***

Appendix: The earthquake history of the Dead Sea environs

Numerous publications list earthquakes that hit the Dead Sea and its surroundings during the last two millennia (e.g. Agnon, 2014; Ambraseys et al., 1994; Ambraseys, 2009; Amiran et al., 1994; Guidoboni et al., 1994, Guidoboni and Comastri, 2005). In Belferman et al. (2018) we adopted from the scores of listed events only the most destructive ones, typically causing local intensities of VII or higher in Jerusalem. For a minimal epicentral distance of 30 km, this would translate to a magnitude of ~5.7 or higher (according to the attenuation relation of Hough and Avni, 2011).

Table A1 lists the Dead Sea earthquakes considered for stress release across the Dead Sea basin during the last two millennia. We used two criteria: noticeable damage in fortified Jerusalem, and seismites in the northern Dead Sea. Our simple model simulates an earthquake time series, given a water level curve. Eleven events from this time series correlate with events of magnitude ~6 or more in the historical record. Yet, the model generates four events that are not included in our original catalog. On the other hand, a single event (~660 CE) listed in Belferman et al. (2018) has no counterpart in the simulations despite a wide range of level curves tested. All these curves are generated by a random number generator, subject to constraints from field data. We first discuss the four events required by the simulations one by one. Then we review the ~660 CE event along with other historical events that were left out already in Belferman et al. (2018).

The earthquakes in Table 1 are classified according to the level of acceptance for being destructive in Jerusalem. The nine events of **Class C** are all consensual, also used by Belferman et al.(2018). These events appear in all catalogs and lists and need no further discussion. The six events of **Class A** are debated events, accepted in the present study. All earthquakes in this class are selected by simultaneously satisfying two criteria: (1) The acceptance regularizes the relation between recurrence intervals and lake level; (2) They are corroborated by evidence from seismites in the northern basin of the Dead Sea (Ein Feshkha and Ein Gedi sites, Fig.A1corroborate).

We chose the year **33** CE to start our simulations. While this earthquake did not cause a widespread damage, it was recorded in all three seismite sites (Kagan et al., 2011), with a maximum of decade uncertainty based on dating by counting lamina under the microscope (Migowski et al., 2004; Williams et al., 2012).

The second entry in Table A1, **~100** CE, refers to two decades of unrest. Migowski et al. (2004) identified a pair of seismites around 90 CE and 112 CE in the ‘Ein Gedi Core. The corresponding

555 sequences in Ein Feshkha and Ze'elim Creek are laminates, attesting to quiescence. A historical
556 hiatus between the Roman demolition of Jerusalem and the erection of Ilya Capitolina in its stead
557 (70-130 CE) preclude historical evidence. Although damage to the Masada fortress has been
558 assigned to an earthquake **1712 CE.**
559 Table A2 lists ten earthquakes that have been reported to damage around Jerusalem but are not
560 required by our simulations. The seven events of **Class R** are the debated events, rejected here
561 after discussion. The three **Class S** events were skipped altogether in that compilation of
562 Ambraseys (2009).
563 Of the seven Class R events, the 7 June **659** CE earthquake was accepted by us in Belferman et al.
564 (2018). The earthquake has been associated with destruction of the Euthymius monastry 10 km
565 east of Jerusalem, but no damage in the town of Jerusalem has been unequivocally reported
566 (Ambraseys, 2009). In Belferman et al. (2018) we included this event in the catalog of Dead Sea
567 earthquakes, as Langgut et al. (2015) have located it on the center of the Jordan Valley segment of
568 the transform (Figure A1). However, this interpretation neglected the possibility that the rupture
569 could have been outside the hydrological effect of the Dead Sea basin. One of the lessons of our
570 numerous simulations is that our model would not support triggering of this earthquake shortly
571 (less than a century) before the mid-8th century crisis, when lake levels were dropping to the lowest
572 point in the studied period (420 m bsl, Figure 1a). When rejecting the 659 CE event, the 419 CE
573 earthquake is the one preceding the mid-8th century crisis; the three century recurrence interval
574 fits well the low lake level.
575 **1016** CE: The collapse of the Dome of the Rock was not explicitly attributed to an earthquake by
576 the original sources, who found it enigmatic as well (Ambraseys, 2009).

1644 CE: Ambraseys (2009) quoted a late Arab author, al-Umari, who reported collapse of houses and deaths of five persons in "the town of Filistin". While Ambraseys has interpreted it probably to Jerusalem, it might refer to al-Ramla, the historical capital of the classical Filistin District, as in "al-Ramla, Madinat Filastin" (Elad, 1992, p335). Or, it is a mistranslation of "Bilad Filistin" which at that time started refer to the entire Holy Land district, without specifying a town (Gerber, 1998). Jerusalem, at that time, was called Bayt el Maqdis or, as nowadays, al-Quds. The only report of an earthquake in Jerusalem around 1644 mentions horror but no structural damage - the 1643 CE event that Ambraseys (2009) tends to equate with the 1644 CE event. A seismite in Ein Gedi core can be correlated with this event (Migowski et al., 2004, Table 2, entry 6). Migowski et al. (2004) have identified the seismite with the 1656 earthquake that was felt in Palestine; Ambraseys' (2009) interpretation was not yet available for them.

1656 CE: This event was strong in Tripoli and only felt in Palestine. Migowski et al. (2004) correlated it to a seismite based on deposition rates (no lamina counting for that interval). Given the 1644 CE entry of Ambraseys (2009), this interpretation should be revised, and the 1656 CE earthquake is not to be associated with any local rupture in the Dead Sea.

Table A1: *A catalog of earthquakes that could potentially damage Jerusalem. The classes denote the level of acceptance of damage to Jerusalem among the researchers: C - consensual; B - accepted by Belferman et al., 2018; A - amended here; R - rejected here.*

Year CE or Century (marked C)	Class	Seismite correl. by site			Reference	Comments
		ZE†	EG¥	EF°		
33	B	+	+	+	MI,K&,W&,	Identified in all three seismites sites, varve-counted to 31 BCE
100~	B	-	2	-	MI,AM	Seismites ~90 and ~112; questionable archaeologic evidence
~175	B	-	+	-	MI	A seismite; no historical or archeological support
363	C	-	-	+	K&,A&	A seiche in the Dead Sea, a seismite at EF° (north Dead Sea)
419	C	+	+	+	KT/MI/K&	
551	A	+	+	+	PA,AM	
747/9,757	C	+	+	+	KT/MI/K&	
1033	C	?	+	+	KT/MI/K&	
~1150	A	+	-	/	AM,K&	I_0 IX - Mar Elias (& Qasr al-Yahud) monastries demolished
1293	C	+	+	+	K&	
1458	C	+	+	hiatus	MI	
1546	C	/	+		MI	
1712	A	/	+		MI	A& / I_0 VII - "ruined three Turkish houses in Jerusalem"
1834	C	+	+		KT,MI	
1903	R	m	m		A&,AM	I_0 VII Mt. of Olives; several shocks, I_0 up to VII over a large area
1927	C	+	+		KT,MI	AV / I_0 VII-VIII in and around Jerusalem (I_0 7.8 by GMPE)

Table A2: *Events listed in some catalogs and subsequently skipped (Class S) or declined (Class D) by Ambraseys (2009), or rejected (Class R) in the present study.*

Year CE	Class	Seismite correl. by site			Reference	Comments
		ZE †	EG¥	EF ◦		
~659	R	-	+	+	L&,AM	Jordan Valley, possibly over 65 km NE of Jerusalem
808	S	/	-	?	A&	
1016	D	?	?	?	AM,A&	Damage to the Dome of Rock, no specific reference to shaking
1042	S	-	+	-	BM	Syria, off the Dead Sea transform
1060	S	/	-	+	A&,SB	The roof of Al-Aqsa collapsed
1063	R				A&,AM,SB	Syrian littoral
1068	D	+	+	+	AM	Neither of the two events can be associated with the Dead Sea
1105	D	?	?	?	A&,AM	"Strong" but "no damage recorded in the sources"
1114	D	+	+	?	A&,AM	1114 - no damage around the city, a swarm, Kingdom's north
~1117	R	+		?	A&,AM	
1557	R				Am	Collapse in Jerusalem: a gun foundry, a forgery, an oven
1644	R	h	+*	h	Am	Some damage and death toll in Palestine, likely Seismite 6 of MI
1656	R	h	-	h	A&,AM,SB	Tripoli VII, Palestine IV, MI misidentified with Seismite 6
1817	R				AM	Two churches damaged in Jerusalem, Holy Sepulchre affected
1870	S	?	-	h	AM	Mediterranean source

Abbreviations and notes:

†ZE - Ze‘ elim Creek; ¥EG - Ein Gedi core; °EF - Ein-Feshkha Nature Reserve

AM: Ambraseys, 2009; A&: Amiran et al., 1994; K&: Kagan et al., 2011; L&: Langgut et al. 2015; KT: Ken-Tor et al., 2004; MI: Migowski et al., 2004; PA: Parker, 1982; W&: Williams et al., 2012.

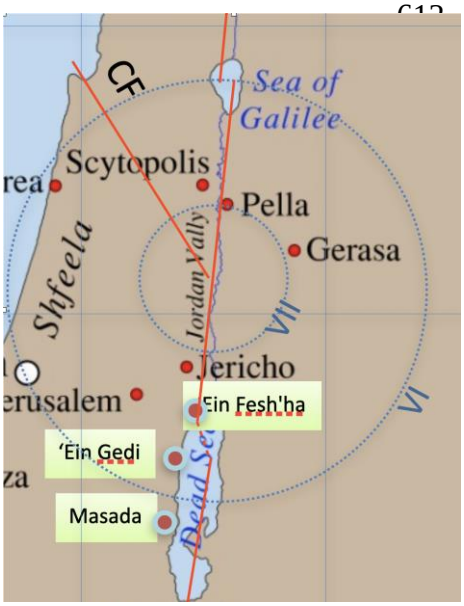

Figure A1: *A map showing the epicenter reconstructed by Langgut et al. (2015) for the* 659/660 CE mainshock.